DURHAM UNIVERSITY

UNDERGRADUATE REVIEW

Surveying Potential Energy Surfaces

Author:

João Luiz MARTINS CARABETTA

Supervisor:

Dr. Halim KUSUMAATMAJA

A review submitted in fulfilment of the requirements

for the degree of Undergraduate in Physics

in the

Simulations of Soft Matter

Centre of Matter Physics

June 28, 2016

DURHAM UNIVERSITY

Abstract

Department of Physics

Centre of Matter Physics

Undergraduate in Physics

Surveying Potential Energy Surfaces

by João Luiz MARTINS CARABETTA

The study of potential energy surfaces underlies a myriad of systems of atoms and molecules such as protein folding, crystals and clusters. Due to its importance, computational methods were developed to characterise these hypersurfaces. I will present the most relevant methods to find the global minima, minimum energy paths and transition states comparing possible implementations of each. Also, the disconnectivity graphs will be introduced as a powerful graph tool to visualise an hypersurface. Finally, I will show how these tools were used to explore the PES of Lennard Jones clusters.

Acknowledgements

Firstly, I have to acknowledge the beauty of the universe randomness. From the distant big bang, through the formation of galaxies, stars systems, planets, life, to the human species, I was lucky enough to be born in the era of science. The era where the rationality is being taken to its extreme and the pursuit for an excellent explanation of reality is a huge institution. Being born this context by pure chance is, of course, the first thing that I have to be grateful of.

People are usually, at least until now, born from other human beings. These people happen to be called parents, usually a man and a woman, whose mine are great. Again, by chance, I was luck enough to be born in an excellent family, that gave me love, care and support whenever I needed, even when I decided to do Physics. For them, Juan and Neire, I own a big part of myself. The other big part goes to my brother, Francisco, that did not let me turn into a boring nerd.

On the science side, I have to be grateful to Halim, the professor that was more like a friend. The guy who listened my ideas with respect and consideration. So, I have to thank him for his openness and competence that he treated me. Also, I have to thank De Koning, that also opened his door and got interested by my ideas.

There is lot of people, colleagues, friends, partners, thinkers that I have to thank, so, to make shorten my speech I will enumerate (with no preference, of course): Descartes, for the scepticism and acceptance of the different, Diego, for being the one that learned with me, Monica, for being the first to open the science doors for me, Duber, my first hard science teacher, Precoce, someone to gossip with, João and Pedro, for exercising my philosophical side and many others that the randomness put me with.

Contents

Chapter 1

Introduction

Most of the atomic and molecular dynamics and structure can be expressed as a manifestation of a potential energy surface (PES). From protein folding and phenomenology of glasses to atomic and molecular clusters physical and chemical properties can be predicted and explained by its PES [38, 6, 11]. It is, by definition, the potential energy of a system as a function of atomic or molecular coordinates [38].

For clusters, the PES is calculated directly using all the coordinates. On the other hand, for biomolecules, glasses and crystals it is expressed as a free energy surface, which just uses a restricted number of parameters. This essay, however, will focus on the analysis of the PES that can be extrapolated to a free energy system. To discuss the theme, some definitions are necessary. I will present them in the further paragraphs.

The electronic degrees of freedom can be neglect by the Born-Oppenheimer approximation. It states that the nuclear motion can be separated from the electronic motion without losing generality on the dynamic behaviour. Although tunnelling effects can be considered, I will not discuss them [38].

The potential energy of a atomic system, V, is a function of the sum of potential energy between atoms of a system, eq.1.1. Thus, the position of the atoms in a 3-dimensional space can be represented by the vector $\mathbf{X} = (\mathbf{x}_1, ..., \mathbf{x}_N)$ that has $3N$ dimensions, being N the number of atoms. In that way, the PES has $3N$+1

dimensions, in which the extra dimension is the potential energy function.

$$V_T(\mathbf{X}) = \sum_{\substack{j,i=1 \\ j \neq i}}^{3N} V(\mathbf{x}_i, \mathbf{x}_j) \tag{1.1}$$

A **stationary point**, SP, in the PES is a configuration where all the nuclear forces vanish, so every component of the gradient vector is zero, $\partial V(\mathbf{X})/\partial \mathbf{x}_\alpha = 0$ with $1 < \alpha < 3N$. To further refine the definition, consider the Taylor expansion of the potential on a SP assuming that the function has continuous second partial derivatives,

$$V(\mathbf{X}) = \frac{1}{2} \sum_{\alpha=1}^{3N} \omega_\alpha x_\alpha^2 + \mathcal{O}(\mathbf{X}^3) \tag{1.2}$$

where $\mathbf{X_0} = \mathbf{0}$ is the stationary point and the zero of energy, $V(\mathbf{0}) = 0$ and $\mathcal{O}(Q^3)$ consists on higher-order terms that can be neglected. The hessian eigenvalue, ω_α, determines the normal mode α of curvature. If $\omega_\alpha > 0$ it means that it is a minimum in the $\mathbf{x}_\alpha$ coordinate, whereas if $\omega_\alpha < 0$ it is a maximum. The number of negative ω_α in a ST is termed index.

A **minima** of a PES is a stationary point with index zero, that means that there is no negative ω_α . At that point any small displacement increases the energy. A **saddle point** is a stationary point with index greater than zero. Hence, the **transition state** is the particular case of a saddle point that has index one [26]. Transition states are important for being the lowest maximum energy point between two minima.

The path that connects the two minima through a transition state is called **minimum energy path** (MEP). This path is given by two **steepest descent path** (SDP) starting from the transition state. A SDP is defined by the direction given by the eigenvector of the smaller positive eigenvalue of the hessian on a given point (Fig.1.1) and it is unique. Said that, there are only one minimum path that connects a transition state to a minimum. So, the minimum energy path

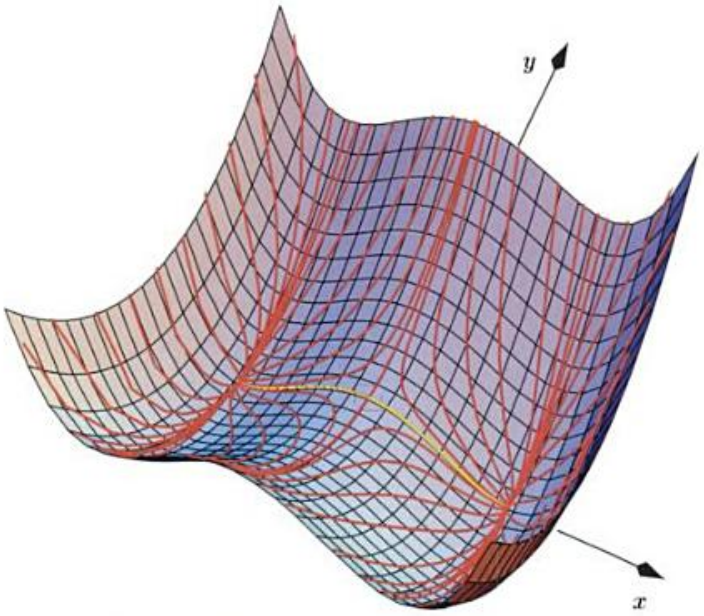

(A)

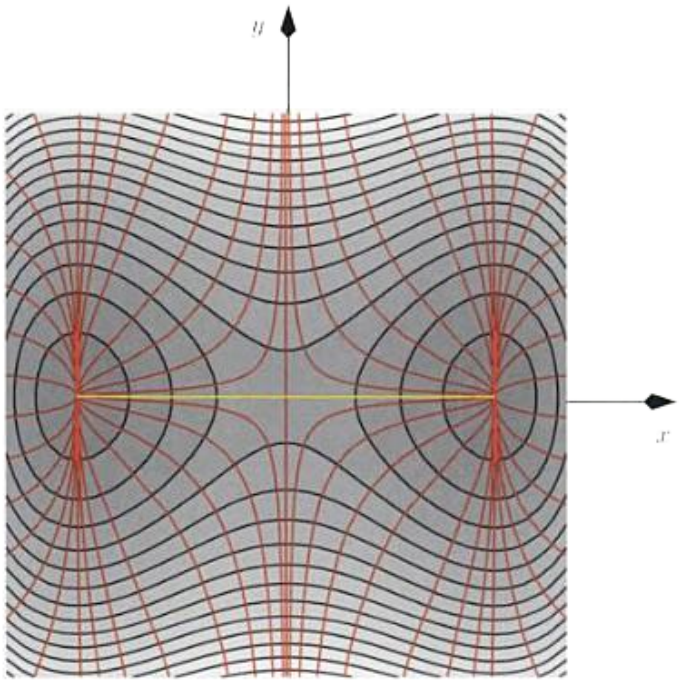

(B)

FIGURE 1.1: Surface (A) and contour (B) plots of the potential surface $V = x^4 - x^2 + y^2$. All coloured lines are steepest descent paths. There are an infinite number of steepest descent paths but only two connects the transition state to the minima which is in yellow. This specific path is called minimum energy path (MEP) (Figures from [38]).

between two minima goes through a transition state by the SDP.

With those definitions, I will show computational algorithms that characterise the PES. First, two important methods, simulated annealing and basin hopping, inspired on statistical mechanics to find the minima will be compared. Second, I introduce two double-ended methods based on nudged elastic bands to find MEPs and transition states. Also, the optimisers have to be explained in order to have a full grasp of the dynamics of the method. Third, I show a powerful graphical tool to structure these information in a appreciable way called disconnectivity graphs. Finally, one famous study case is analysed to demonstrate the power of these tools, the Lennard Jones clusters, in which all presented methods are used, .

-

Chapter 2

Global Optimisation

2.1 Introduction

The global optimisation problem is a topic of great interest, thus very active [37, 39]. Optimised methods allow companies to cut costs and improve performance in problems such as the active structure of a biomolecule, the design of computers and microprocessor circuits [19]. For instance, if the global minimum of the primary amino acid sequence could be found, it would give precious insights about protein folding and save laboratory time. Several approaches to find global minima have been suggested but this work will focus in unbiased methods.

These type of methods have the advantage of being transferable between different systems. Although, it is usually not as fast as a biased method, where prior knowledge of the system is demanded, further implementations can combine both to achieve better results [23]. Many other unbiased methods were proposed, the multiple images of the system [30] , interval arithmetic [17] , taboo searches [13] and methods based in changes of dimension [7].

I will concentrate on two unbiased methods the Simulated Annealing [19] and the stochastic Basin Hopping [37] . The former for its historical importance of being the first global optimisation algorithm to be generally applicable [39, 19]. The latter for its success on finding global minima for a wide range of

systems.

2.2 Simulated Annealing

Inspired in statistical mechanics, Kirkpatrick, Gelatt, and Vecchi proposed a minimisation algorithm that mimics the annealing process [19] .One of the central questions of statistical mechanics is the behaviour of a system at very low temperatures, $\mathbf{T} \sim 0K$. Differently from high temperatures, at low temperature conditions low energy state or states dominate the system properties. To reach ground states experimentally the temperature has to be lowered down slowly, then it has to be kept to almost zero for a while. For instance, this annealing process can be used to find the stable configuration of a crystal. But, if its not well controlled, the crystal can reach *metastable* configurations, present defects or not form.

This idea can be used to minimise combinatorial systems. It can be done by replacing the energy for a cost function and the temperature is introduced at the choosing parameter. A pseudocode go as follows:

- $\mathbf{X}_{min} =$ pick random $\mathbf{X}$
- For T from $T_{initial}$ until 0:
  - $\mathbf{X}_{new} =$ pick random $\mathbf{X}$
  - If $E(\mathbf{X}_{new}) < E(\mathbf{X}_{min})$ or $P(E(\mathbf{X}_{new}, E(\mathbf{X}_{min}), T) <$ random $[0, 1]$:
    - $\mathbf{X}_{min} = \mathbf{X}_{new}$
- Output $\mathbf{X}_{min}$

where $\mathbf{X}$ is a configuration of the system, E is the cost function chosen to minimised and T is a variable that does the temperature role on the minimisation. The temperature goes from a initial value greater than zero to zero in a

step that can be adjusted. One good approach is to use $T_{step} = T_{initial}/n$ with n being the number of runs. This guarantees that the temperature will decrease slowly at low temperatures.

There are two condition to select a new minima. The first, $E(\mathbf{X}_{new}) < E(\mathbf{X}_{min})$ is the most obvious one. However, if it used alone, the annealing is too fast, increasing the chance of reaching a *metastable* minima. For that reason, the second condition, $P(E(\mathbf{X}_{new}, E(\mathbf{X}_{min}), T) <$ random $[0, 1]$, is necessary. It says that if the new energy is greater than the original one, $E(\mathbf{X}_{new}) > E(\mathbf{X}_{min})$, there is a chance between a random number between 0 and 1 (generated by a uniform distribution) of accepting the new configuration. The function usually used to calculate the probability, $P(E(\mathbf{X}_{new}, E(\mathbf{X}_{min}), T)$ was introduced by Metropolis et al. [24] to simulate a collection of atoms at equilibrium at a temperature. The probability is,

$$P(E(\mathbf{X}_{new}), E(\mathbf{X}_{min}), T) = exp((E(\mathbf{X}_{min}) - E(\mathbf{X}_{new}))/T), \tag{2.1}$$

which resembles the Boltzmann probability factor, $exp(-E(\mathbf{X})/kT)$, not by chance. It simulates the thermal fluctuations of atoms in a thermal bath.

This algorithm proved to be very powerful for combinatorial minimisation. A classic example is the traveller salesman problem. The problem consists to find the minimum distance that connects a set of points N (cities) in an area. The Figure 2.1 was taken from Kirkpatrick, Gelatt, and Vecchi original paper to demonstrate the potential of the method on that problem. The figure shows 4 square areas with 400 cities, N, divided in 9 clusters. Each subfigure corresponds to a temperature that is decreased until it reaches zero, being the upper left the highest temperature, $T = 1.2$ and the lower right the lowest. The effect of the algorithm can be seen by comparing them, the former presents a dense path with several line crosses whereas the latter has a clearer path with no intersections.

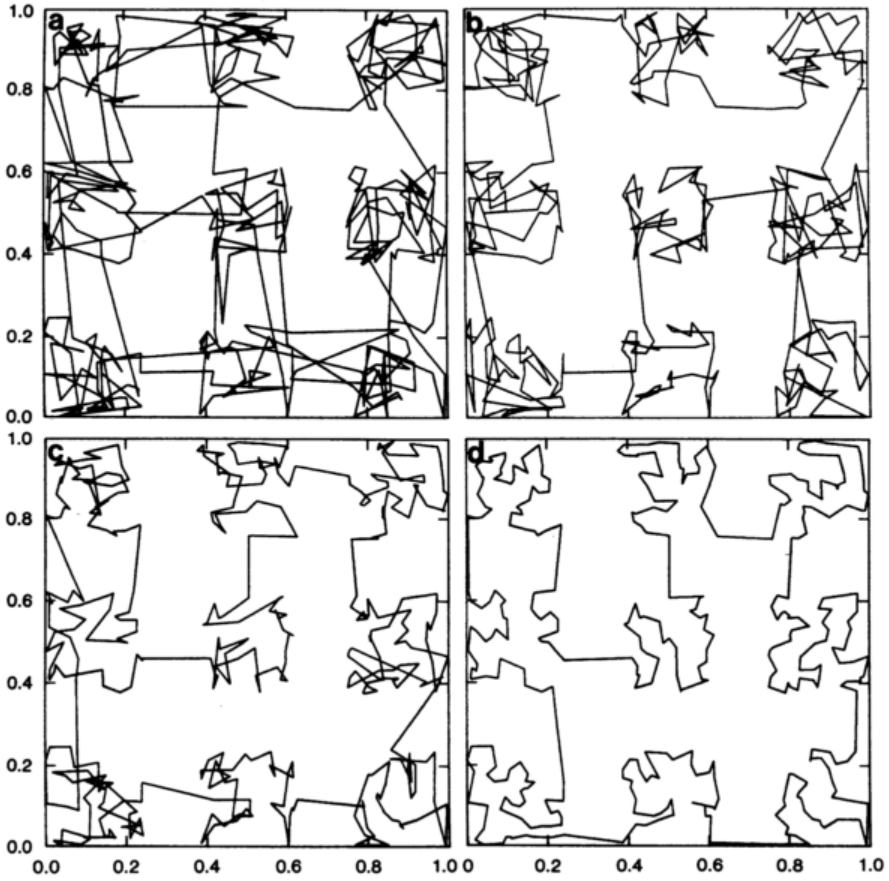

FIGURE 2.1: Results of a 400 cities travelling salesman problem where the points are distributed in nine regions. (a) T=1.2, $\alpha = 2.0567$; (b) T=0.8, $\alpha = 1.515$; (c) T=0.4, $\alpha = 1.055$; (d) T=0.0 $\alpha = 0.7839$ (Figure from [19])

A more precise way to measure the efficiency of the method is by the average step between cities is $\alpha = D/N$, where D is the total path. It is known that the shortest closed path through the points in a area A is around $D\ \sqrt{AN}$, for large N [1] . If we choose the length of the side of the square to be $\sqrt{N}$, thus the average step expected is $\alpha \sim 1$.

The Figure 2.1 shows that α drops significantly with temperature T. It reaches $\alpha = 0.7839$ with $T = 0.0$, demonstrating that the closed path achieved by the simulated annealing algorithm reached a solid minima.

Although being used at great diversity of problems with modifications or not, it was proved to be quite unsuccessful at minimising atomic structures such as the Lennard Jones cluster [37]. Some tries achieved an unstable minimisation

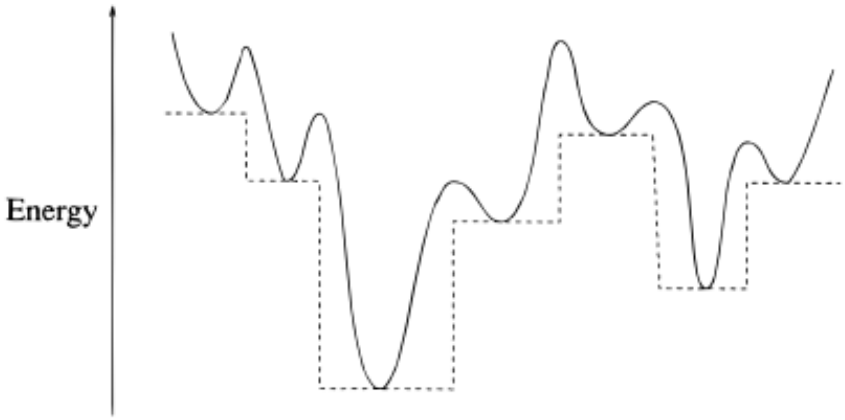

FIGURE 2.2: A diagram that demonstrate how the transformation affects the energy. The solid line is the original energy and the dashed line is the modified energy.(Figure from [37])

up to LJ_{19} besides the fact it did not provided a good set of local minima of the system [29, 34]. In order to solve the LJ clusters global minimisation challenge, Wales and Doye proposed the following method.

2.3 Basin Hopping

The Basin Hopping method was proposed to solve global minimisation problems for cases that Simulated Annealing [37]. The process of the algorithm is similar, there is a random displacement that is then chosen according to the Metropolis rule. There are two key differences. First, the random displacement is restricted to the neighbourhood of the current position, $\mathbf{X}_{min}$, using the Monte Carlo method. It just perturbs the current coordinates slightly. Second, the random displacement is minimised. This means that the Potential Energy Surface (PES) being analysed is actually,

$$\tilde{\mathbf{E}}(\mathbf{X}) = min(E(\mathbf{X})). \tag{2.2}$$

This is an important modification to the PES that transforms a continuous

surface in a discrete surface. An one dimensional example (Fig. 2.2), the continuous function turns into a series of plateaus, what is also called basin attractors. With this modification, atoms can swap places without encountering ultra high energy barriers. Thus, the pseudo-algorithm for this method is,

- $\mathbf{X}_{min} =$ min(pick random $\mathbf{X}$)
- Do n_{steps} at $T = T_{constant}$:
  - $\mathbf{X}_{new} =$ min(MC($\mathbf{X}_{min}$))
  - If $E(\mathbf{X}_{new}) < E(\mathbf{X}_{min})$ or $P(E(\mathbf{X}_{new}), E(\mathbf{X}_{min}), T) <$ random $[0, 1]$:
    - $\mathbf{X}_{min} = \mathbf{X}_{new}$
  - If convergence tolerance reached: stop
- Output $\mathbf{X}_{min}$

Here, the min() notation means the minimisation of configuration $\mathbf{X}$ using a optimiser (see Chapter 3). The convergence tolerance can be adjusted in respect with the problem being solved, it can be the energy difference between consecutive configurations, for instance. Also, MC is a canonical Monte Carlo random displacement of the coordinates of configuration $\mathbf{X}_{min}$ restricted to a certain range. The Metropolis algorithm is used to choose whether the new minima is going to be selected. It is important to highlight that the temperature in the original implementation [37] was kept constant, hence the allowed step between plateaus was also constant. The number of Monte Carlo steps was already predefined.

2.4 Conclusion

This chapter presented two unbiased methods to find global minimum in combinatorial systems. The first introduced, the simulated annealing, is based on

a statistical mechanical process of annealing. It solves with great success the traveller salesman problem for 400 cities, which was undone at the time of the proposal of the algorithm. The basin hopping method is based on the idea of temperature and randomness of the former, but it includes a field transformation to solve global optimisations for complicated surfaces. This method proved to be very successful as we will see in Chapter 5.

Chapter 3

Double Ended String Based Path Methods

3.1 Introduction

This section will present a chain-of-state method for double-ended situations based on an elastic band to find Minimum Energy Paths (MEP) between two minima states. As a consequence of finding the MEP, the location of the saddle point which gives a global view of the energy landscape is established. The saddle point is a very important information, for instance, to estimate the transition rate within harmonic transition state theory (hTST)[16, 15, 18].

The transition state theory (TST) attempt to predict the transition rates between a reactant and a product using statistical mechanics [15]. It assumes that there is a dividing surface with $D-1$ dimensions, with D the number of degrees of freedom in the system, in which the system is equally likely to relax either to the reactants or products. In a crystal, the tightly packed structure of atoms allows an harmonic approximation, so called harmonic transition state theory (hTST). In that case, the dividing surface becomes the transition state that is the central information to calculate the transition rate [38]. This theory can be used to study the diffusion of a Pt island in a Pt(111) surface [15], the dissociation of CH_4 on Ir(111) [16] or isomerisation of $(H_2O)_9$ [38].

There are several other methods developed to either find just the saddle point or to find the MEP. Those methods can rely just on the interpolation between the initial and final value such as the LST (straight line) or QST (parabola) [33, 14]. But those methods are limited to very simple configurations, restricting their actual use for better initial guesses for more advanced methods. Other approaches using a string of state images with no elastic band were tried but they either require very good initial guesses of the MEP or present a serious sliding down problem [15, 10, 8, 35, 5].

The method that I chose to discuss is the Nudged Elastic Band (NEB). This is a method with a fairly easy implementation but robust. It just uses the position, energy and first derivative of the images to successfully find the MEP for complicated multidimensional problems. Also, it is widely used in material sciences, chemistry and biodynamics [33, 22], highlighting the strength and versatility of the method.

Since it is a dynamic method that has to find the (nearest) minimum structure from a starting position, some optimisation methods for this search were developed. So, I will refer to an optimisation method as *optimiser*.

First, I will present the NEB method following its historical developments, justifying the structure of the method[16, 15, 18] . Then, I introduce the Doubly NEB which is a variation intended to deal with better optimisers at high energies configurations. After that, some relevant optimisers are covered highlighting their ideas of minimisation. Finally, I compare combinations of the NEB/DNEB with several optimisers.

3.2 Nudged Elastic Band (NEB)

The Nudged Elastic Band Method (NEB) consists in a string of states of the system (images) that are connected by springs in order to provide a discrete representation of a path from the initial configuration (**I**) to the final configuration (**F**) [16, 15]. Its initial interpolation is usually made in the cartesian distance between **I** and **F**. For more specific cases the initial interpolation may need a better guess. A string of N+1 images have its first and last images fixed because $\mathbf{X}_0 = \mathbf{I}$ and $\mathbf{X}_N = \mathbf{F}$. In that way, just N-1 images are movable, thus, subject of an optimisation. However, all images are bound in some way by those two fixes images by a spring potential that connects the images in serie,

$$\tilde{V} = \frac{1}{2}k\sum_{i=1}^{N}(\mathbf{X}_i - \mathbf{X}_{i-1})^2, \tag{3.1}$$

with k being an adjustable variable that resembles the elastic coefficient. Then, an optimisation algorithm relax this string towards the MEP using a combination of the true potential and the NEB spring potential. Therefore, the potential equation that describe the movable system is,

$$\mathbf{S}(\mathbf{X}_1, ..., \mathbf{X}_{N-1}) = \sum_{i=1}^{N-1} V_T(\mathbf{X}_i) + \frac{1}{2}k\sum_{i=1}^{N}(\mathbf{X}_i - \mathbf{X}_{i-1})^2. \tag{3.2}$$

However, there are some problems that arise from the implementation of eq.3.2. When the MEP is curved, the spring force gets fairly perpendicular to the MEP, pulling the elastic bands off and corner cutting the MEP (Figure 3.1). Also, the images slide down towards the endpoints, **I** and **F**. It decreases the image density at the saddle point region, where it is most needed, due to the parallel force of the true force [16, 15, 33] Those problems cannot be solved by adjusting the elastic coefficient, k, because the forces are correlated. So, although increasing k minimises the sliding down issue, it exacerbates corner

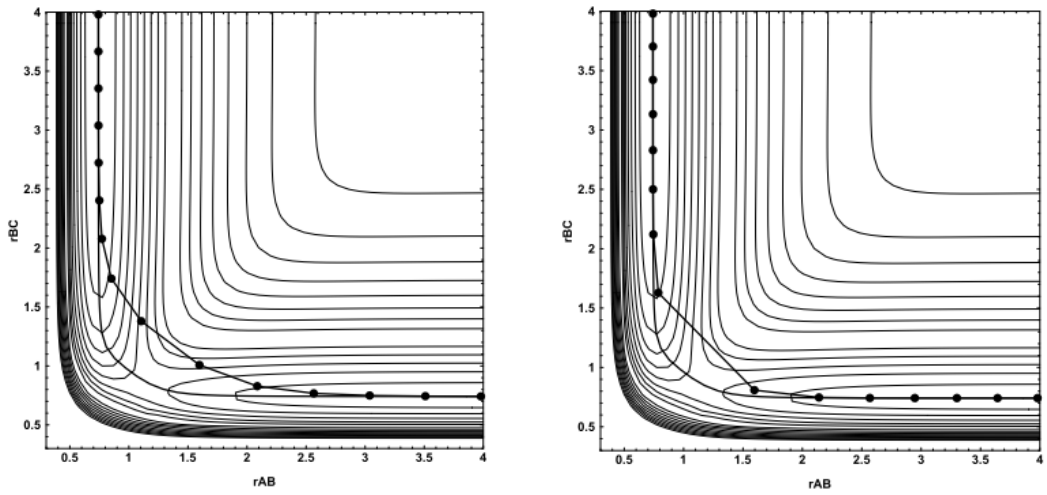

(A) (B)

FIGURE 3.1: A contour plot of LEPS potential with horizontal axis being the distance of atom A-B and vertical axis the distance of B-C. The plot shows a plain elastic band with filled circles and a solid line. (A) The elastic coefficient k is 1.0, which leads to an overestimation of the saddle point. (B) Here $k = 0.1$ that reduces the corner cutting, but slides the images towards the minima decreasing the resolution on the saddle point(Figures modified from [18]).

cutting. The solution then is to 'nudge' specific components of the vectors. If we take just the parallel component of the spring force, $\tilde{\mathbf{F}}^{\parallel}$ and the perpendicular component of the true force, $\mathbf{F}^{\perp}$, the total force experienced by each image is,

$$\mathbf{F}_i^{NEB} = \mathbf{F}_i^{\perp} + \tilde{\mathbf{F}}_i^{\parallel}. \tag{3.3}$$

where the true force is given by

$$\mathbf{F}_i^{\perp} = -(\nabla V(\mathbf{X}_i) - \nabla V(\mathbf{X}_i) \cdot \hat{\boldsymbol{\tau}}_i), \tag{3.4}$$

with $\hat{\tau}_i$ being the unit component of the tangent (that will be explained soon) and the spring force as

$$\tilde{\mathbf{F}}_i^{\parallel} = k(|\mathbf{X}_{i+1} + \mathbf{X}_i| - |\mathbf{X}_i + \mathbf{X}_{i-1}|)\hat{\boldsymbol{\tau}}_i. \tag{3.5}$$

The absolute value of the distances in the equation above guarantees equally

spaced images in regions of high curvature (see fig 3.3) when the angle between $\mathbf{X}_{i+1} + \mathbf{X}_i$ and $\mathbf{X}_i + \mathbf{X}_{i-1}$ is high [16].

The most simple approach to calculate the tangent at an image *i* is to use the adjacent images $\mathbf{X}_{i+1}$ and $\mathbf{X}_{i-1}$,

$$\boldsymbol{\tau} = \mathbf{X}_{i+1} - \mathbf{X}_{i-1}, \tag{3.6}$$

or in a better way,

$$\boldsymbol{\tau} = \frac{\mathbf{X}_{i+1} - \mathbf{X}_i}{|\mathbf{X}_{i+1} - \mathbf{X}_i|} + \frac{\mathbf{X}_i - \mathbf{X}_{i-1}}{|\mathbf{X}_i - \mathbf{X}_{i-1}|}, \tag{3.7}$$

that is then normalised to $\hat{\boldsymbol{\tau}} = \boldsymbol{\tau}/|\boldsymbol{\tau}|$. This slightly improved tangent also ensures that the images will be equidistant at high curvature regions.

However, this implementation forms kinks that are shown in figure 3.3. The NEB with seven movable images was linearly interpolated between the two ends . The surface is a combination of a LEPS potential and an harmonic oscillator [16, 18]. The images were minimised using the Velvet algorithm (that will be discussed later on). They converged toward the MEP by the action of the total force, $\mathbf{F}_i^T$, but the magnitude of the force stops dropping at a certain number of interactions. The images oscillates in regions of inflection point of the MEP, due to the larger magnitude of the parallel force compared to the perpendicular force. These kinks do not vanish after a considerable high number of interactions. Thus, this effect prevents the method to find a good approximation of the MEP in some cases.

In order to solve this problem, a switch function was added when the angle between $\mathbf{X}_{i+1}$ and $\mathbf{X}_{i-1}$ was high, adding a fraction of the perpendicular spring vector component. But it led to an overestimation of the saddle point, what is inconvenient in most cases [16]. The approach that successfully diminished the kinks changed the tangent definition.

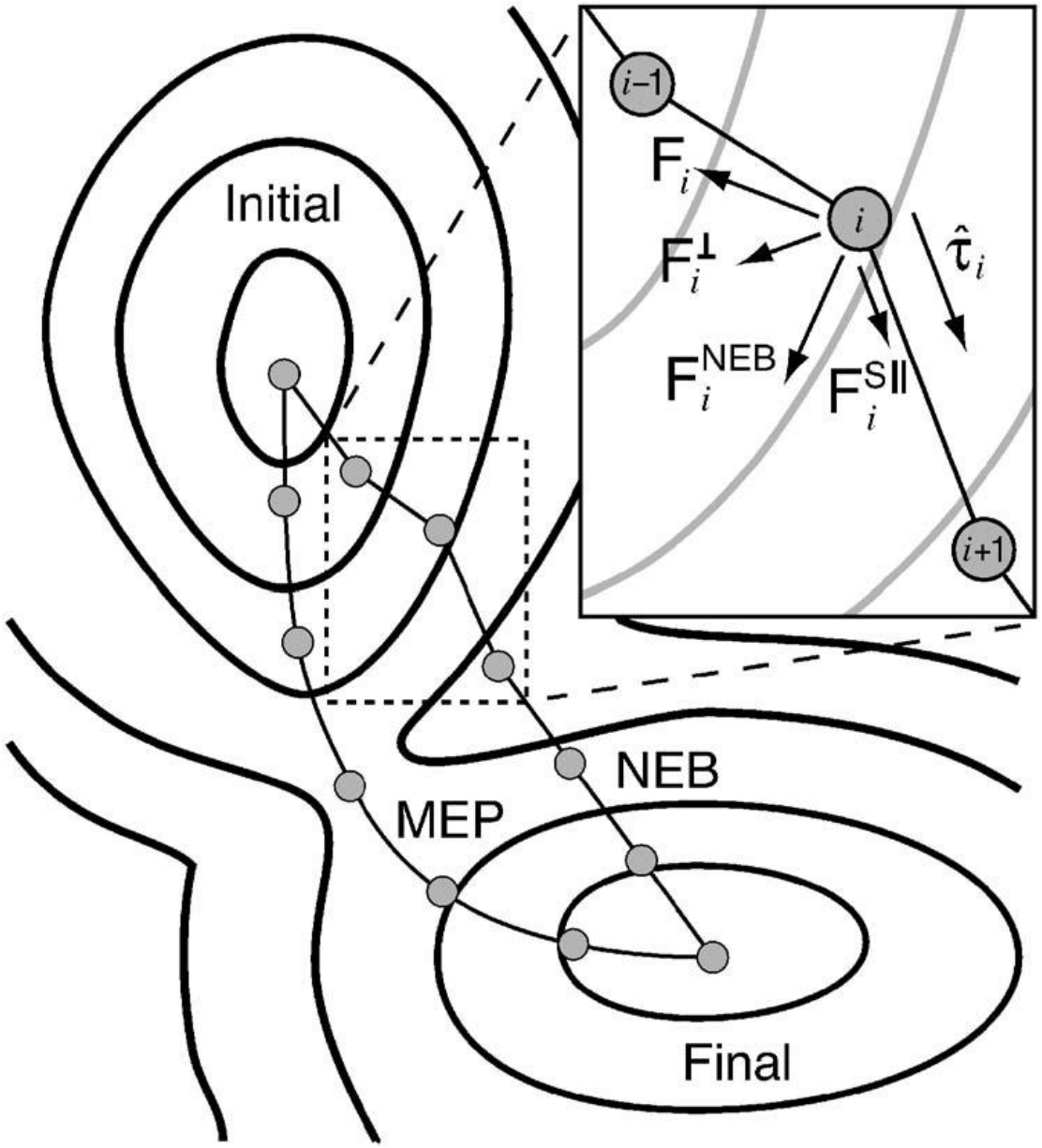

FIGURE 3.2: Implementation of the Nudged Elastic Band (NEB) in a hypothetical situation. A spring with 5 movable images is disposed between the Initial and Final configurations. There are two strings, the NEB is the active string that was just released whereas the MEP string already found the MEP. The zoomed part shows the vectors configuration in an image, *i*. The tangent is $\hat{\tau}$ and the total true force is F_i. Thus, the perpendicular component of the true force is $F_i^{\perp}$ and the parallel component of the spring force is $\tilde{F}_i^{\parallel}$ resulting in the NEB force $\mathbf{F}_i^{NEB}$, that is the force acting in the image.

It is important to note that $\mathbf{F}_i^{NEB}$ is pointing towards the MEP (Figure from [31]).

The new tangent instead of using both adjacent images uses the higher energy image [16]. Then the tangent is,

$$\boldsymbol{\tau} = \begin{cases} \boldsymbol{\tau}_i^+ = \mathbf{X}_{i+1} - \mathbf{X}_i & if \quad V_{i+1} > V_i > V_{i-1} \\ \boldsymbol{\tau}_i^- = \mathbf{X}_i - \mathbf{X}_{i-1} & if \quad V_{i+1} < V_i < V_{i-1} \end{cases} \tag{3.8}$$

where V_i is the energy of the image i, $V(\mathbf{X}_i)$ and the tangent has to be further normalised. If both energies, V_{i+1} and V_{i-1} are greater or lower than V_i, the tangent is the weighted average of the neighbouring images. This plays a role in situations where the central image, V_i, is on a saddle point or a minima, reducing the chance of an abrupt change of tangent. Thus,

$$\boldsymbol{\tau} = \begin{cases} \boldsymbol{\tau}_i^+ \Delta V_i^{max} + \boldsymbol{\tau}_i^- \Delta V_i^{min} - & if \quad V_{i+1} > V_{i-1} \\ \boldsymbol{\tau}_i^+ \Delta V_i^{min} + \boldsymbol{\tau}_i^- \Delta V_i^{max} - & if \quad V_{i+1} < V_{i-1} \end{cases} \tag{3.9}$$

where,

$$\Delta V_i^{max} = max(|V_{i+1} - V_i|, |V_{i-1} - V_i|) \tag{3.10}$$

and

$$\Delta V_i^{min} = min(|V_{i+1} - V_i|, |V_{i-1} - V_i|) \tag{3.11}$$

This implementation guarantees that the NEB will converge to the MEP for any given set of movable images. The motivation for that choice of tangent comes from different methods to find the MEP from a saddle point. Given the saddle point, a displacement of the system is done and the energy is minimised conserving the distance from the saddle point. This will give a point in the MEP, M1. Then, from M1, the procedure is repeated until a minimum is found. It is known that the MEP can just be found going downwards in energy, if one starts on a minima it will not converge to a saddle point. Therefore, the choice

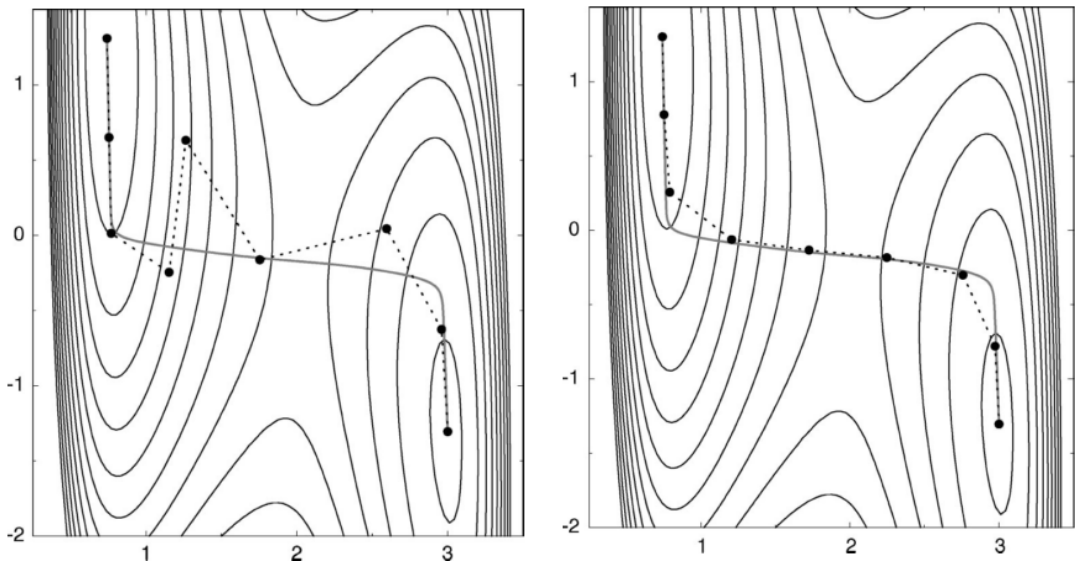

(A) (B)

FIGURE 3.3: Comparison of the NEB implementation between the original tangent estimative (A) and the modified tangent implementation (B). The surface is a combination of a LEPS potential and an harmonic oscillator. (A): It is clear that the images (solid dots) have a limited convergence to the MEP (solid line), creating kinks that oscillate indefinitely. (B): The modified tangent implementation stabilises the images reaching a more precise MEP estimative (Figures from [16].

for a tangent that follows the MEP downwards will use this procedure in with all images once the saddle point is stablished.

However, when Maragakis et al. applied this method in wide range of problems, it showed to be not stable for more powerful optimisers [22] . It was found later that it was due to extra parameters introduced by the springs [33].

3.3 Doubly Nudged Elastic Band (DNEB)

The Doubly Nudged Elastic Band (DNEB) method was proposed by Trygubenko and Wales to improve the convergence of the NEB for faster optimisation methods (that will be discussed in the following subsection), more specifically the L-BFGS [33]. The authors found an instability problem with the minimisation of an LJ_7 cluster when it is minimised with the L-BFGS method if the overall

rotation and translation (ORT) of the system is not eliminated. By experimentation, the problem with the NEB arises due to the complete removal of $\tilde{\mathbf{F}}^{\perp}$. Hence, they proposed that the force that acts at an image should be,

$$\mathbf{F}_i^{DNEB} = \mathbf{F}_i^{\perp} + \tilde{\mathbf{F}}_i^{\parallel} + \tilde{\mathbf{F}}_i^{*} \tag{3.12}$$

where the $\tilde{\mathbf{F}}_i^{*}$ is a term that contains a proportion of the $\tilde{\mathbf{F}}_i^{\perp}$. First, they proposed $\tilde{\mathbf{F}}_i^{*} = \xi\tilde{\mathbf{F}}_i^{\perp}$, which had good results if ξ had values between 0.1 and 0.01. However, besides adding a new variable ξ, it is unstable when $\xi\tilde{\mathbf{F}}_i^{\perp}$ and $\mathbf{F}_i^{\perp}$ have comparable magnitudes. It creates instabilities similar to what was seen with the implementation of eq. 3.2, generating some corner cutting. Since that problem was solved by 'nudging' the components, the following equation was suggested,

$$\tilde{\mathbf{F}}_i^{*} = \tilde{\mathbf{F}}_i^{\perp} - (\tilde{\mathbf{F}}_i^{\perp} \cdot \hat{\mathbf{F}}_i^{\perp})\hat{\mathbf{F}}_i^{\perp}. \tag{3.13}$$

This implementation improves considerably the stability of the NEB method (see Table 3.1) along the L-BFGS, even better if the initial path presents high forces [32], however, it does not converge exactly to a MEP. The problem arises because when a NEB converges, the $\mathbf{F}_i^{\perp}$ goes to zero. However, in order to get $\tilde{\mathbf{F}}_i^{*}$ to zero the $\tilde{\mathbf{F}}_i^{\perp}$ should be parallel to $\mathbf{F}_i^{\perp}$, what does not happen in curved regions. Therefore, the DNEB method presents a limited convergence towards the MEP [32]. Figure 3.5 (A) demonstrates this effect in which the DNEB presents an oscillatory behaviour when it reaches a certain force.

Both Trygubenko and Wales and Sheppard, Terrell, and Henkelman used a switch function from DNEB to NEB according to some convergence variable [32, 33] This allowed the string to stabilise in the MEP thus giving a better estimative of the path.

3.4 Optimisers

The NEB and DNEB method presented above use a force projection to move images towards a MEP and a saddle point. Thus, I will present some force-based optimisers that play a central role in these methods optimisation. The optimisers are organised according to their minimisation power, from the lowest to the highest.

3.4.1 Steepest Descents

The simpler method to minimise a system is the Steepest Descents[32]. I am presenting it as a base of comparison for the following ones. Based on the newtonian dynamics, it completely quench the momentum of the image ignoring the velocity factor. Then, a given configuration $\mathbf{X}(t)$,

$$\mathbf{X}(t+1) = \mathbf{X}(t) + \alpha\mathbf{F}(t) \tag{3.14}$$

where α is an adjustable constant and $\mathbf{F}(t)$ is the force component. If α is negative, the image will converge to a minimum. This method does not take advantage of the velocity that the image can have towards a MEP, depending only on the force projection.

3.4.2 Slow-Response Quenched Velocity Velvet

The Slow-Response Quenched Velocity Velvet (SQVV) was developed by a modification of a previous Velocity Velvet (VV) optimiser that is used in molecular dynamics to stabilises the convergence of the NEB [33]. It also uses Newtonian Dynamics, but it takes advantage of the velocity of the image. The formulation is,

$$\mathbf{X}(t+1) = \mathbf{X}(t) + \alpha\mathbf{V}(t) - \alpha\mathbf{F}(t) \tag{3.15a}$$

$$\mathbf{V}(t) = (\mathbf{V}(t) \cdot \hat{\mathbf{F}}(t))\hat{\mathbf{F}}(t) \tag{3.15b}$$

$$\mathbf{V}(t+1/2) = \mathbf{V}(t) - \alpha\mathbf{F}(t) \tag{3.15c}$$

$$\mathbf{V}(t+1) = \mathbf{V}(t+1/2) - \alpha\mathbf{F}(t+1) \tag{3.15d}$$

here α is also an adjustable constant, $\mathbf{V}(t)$ is the velocity at state t. This formulation uses the velocity related to gradient to increase the speed of convergence. The modification done from the VV is at eq. 3.15b that quench the perpendicular component of the velocity vector in relation to the force [33]. The quenching in any other order in the algorithm was tested by Trygubenko and Wales with no better results.

There is a very similar method that takes an similar approach of quenching the velocity called quick-min. The only difference is that it zeros the velocity vector if it is opposed to the force [18, 32]

3.4.3 Fast Inertial Relaxation Engine

The Fast Inertial Relaxation Engine (FIRE) like SQVV uses the velocity to help find the minimum [32, 3] . The main differences are that FIRE zeros the velocity if it is opposite to the force and it only takes a part of the force direction into the velocity vector, that conserves momentum in other directions. Given the initial values of the time step Δt, the variable $\alpha = \alpha_{start}$, the velocity vector $\mathbf{V} = 0$ and a initial position $\mathbf{X}(t)$, the implementation is,

$$P(t) = \alpha \mathbf{F}(t) \cdot \mathbf{V}(t), \tag{3.16a}$$

$$\mathbf{V}(t+1) = (1-\alpha)\mathbf{V}(t) + \alpha \hat{\mathbf{F}}(t)|\mathbf{V}(t)|, \tag{3.16b}$$

$$if \quad P(t) > 0 \longrightarrow \begin{cases} \Delta t(t+1) = min(\Delta t(t) f_{inc}, \Delta t_{max}), \\ \alpha(t+1) = \alpha(t) f_{\alpha}, \end{cases} \tag{3.16c}$$

$$if \quad P(t) \leq 0 \longrightarrow \begin{cases} \Delta t(t+1) = \Delta t(t) f_{dec}, \\ \alpha(t+1) = \alpha_{start}, \\ \mathbf{V}(t+1) = 0. \end{cases} \tag{3.16d}$$

$$\mathbf{X}(t+1) = \mathbf{X}(t) + \alpha \mathbf{V}(t) \tag{3.16e}$$

where $\mathbf{V}$ is the velocity vector, $\mathbf{P}$ is a The constants can be for most cases set as $f_{inc} = 1.1$, $f_{dec} = 0.5$, $\alpha_{start} = 0.1$ and $f_{\alpha} = 0.99$, hence the only adjustable variable is Δt_{max}. The equation 3.16e can be substituted for any other integrator. This is a fast method that is robust to multidimensional systems and it does not imply complex coding for implementation [3].

3.4.4 Limited-memory Broyden-Fletcher-Goldfarb-Shanno

The Limited-memory Broyden-Fletcher-Goldfarb-Shanno (L-BFGS) is a method that estimates the second derivative to use this information to go towards an harmonic minimum [32, 27]. It construct the inverse Hessian matrix $\mathbf{H}^{-1}$ from a diagonal matrix (The Hessian matrix construction is out of scope of this project, for more information check ref.[27]). There are two variations of that method. The first called L-BFGS(line) its implementation is basically,

$$\mathbf{d}(t) = \mathbf{F}(t)\mathbf{H}^{-1}(t), \tag{3.17a}$$

$$\mathbf{X}(t+1) = \mathbf{X}(t) + \alpha\mathbf{d}(t), \tag{3.17b}$$

where $\mathbf{d}(t)$ is the search direction and α is an adjustable constant.

The second do not do the line search hence being called L-BFGS(hess),

$$\mathbf{X}(t+1) = \mathbf{X}(t) + \mathbf{F}(t)\mathbf{H}^{-1}(t), \tag{3.18a}$$

an implementation that depends on the correct guess of the initial Hessian. If it gives too large values it results in oscillatory or chaotic behaviour, whereas small values converge too slow.

3.4.5 GL-FBGS

The Global L-FBGS (GL-FBGS) has a similar idea of the previous one but it builds a Hessian for all the images at once instead of optimising each image independently [32, 4]. Hence, the dimensionality of the matrix goes from $3 \times A$ for the L-FBGS, to $3 \times A \times N$ for the GL-FBGS where A is the number of atoms and N is the number of images. Thus, the two variations described above are valid GL-FBGS(line) and GL-FBGS(hess), the change is that the vectors are $\mathbf{X} = (\mathbf{X}_1, \mathbf{X}_2, ..., \mathbf{X}_N - 1)$ and $\mathbf{F} = (\mathbf{F}_1, \mathbf{F}_2, ..., \mathbf{F}_N - 1)$.

3.5 Comparison

This section compares both elastic band methods DNEB and NEB using different optimisers that were presented in the last section. It is important to keep in mind that comparisons of double ended methods are bound to errors since a

TABLE 3.1: Number of iterations for each connected path of permutations of atoms of the LJ_7 cluster with a 50-image string. The numbers represent the atoms labeled in Figure 5.2

Method	1-2	2-3	3-4	4-5
DNEB/L-BFGS(hess)	131[a]	439	171	326
DNEB/SQVV	1130	15178	2777	23405[b]
NEB/SQVV	11088	—[c]	30627	—[c]

[a] The number of iterations is the sum of SQVV to initialise the string (around 100) with the L-BFGS.
[b] This value is not significant because the NEB found a different MEP
[c] A MEP was not found

string can converge to different MEPs [33]. Also, the termination criteria chosen to stop the convergence can influence the interaction number, therefore changing some of the results. Regardless of that, I choose two comparisons, one that shows the great advantage of the DNEB over the NEB using the L-BFGS at high initial forces and introduce the connected path concept; the other that compares a wide range of optimisers with the NEB and the DNEB giving a broader idea of the speed of each combination.

The efficiency of the DNEB over NEB can be seen in Table 3.1. It shows the number of iterations of an 50 images string to find the MEP of a Lennard Jones cluster of 7 atoms (LJ_7). The minimisation connected 5 minima in the path and each path MEP between given minima is represented on the table. This configuration usually presents high initial force values, being a good test for the DNEB method. The criteria chosen to stop convergence in that case was the root-mean-square of the perpendicular component of the force,

$$\mathbf{F}^{\perp}_{RMS} = \sqrt{\frac{\sum_{i=1}^{N} |\mathbf{F}^{\perp}_{i}|}{N\eta}}, \tag{3.19}$$

where N is the number of images and η is the number of atomic degrees. So, the convergence stopped then $\mathbf{F}^{\perp}_{RMS} < 0.01$.

The results show that the DNEB/L-BFGS is one order of magnitude faster

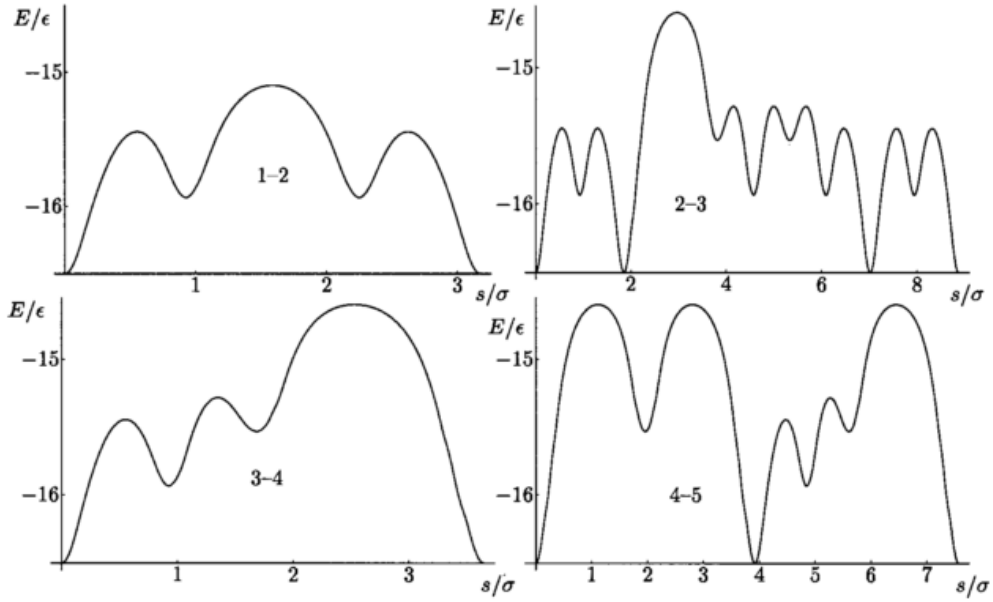

FIGURE 3.4: Energy as function of the path length, s, of connected paths of permutations of the LJ_7 cluster. The numbers 1-2, 2-3, 3-4 and 4-5 represent permutation of these atoms labeled in Figure 5.2A. These paths were done using the NEB method with its variations that were further refined by the EF method (see next section). (Figure from [31]).

than the other approaches. Also, only the DNEB method found connected pathways, minima that have two paths from transition states and transition states that have two paths to minima, in all the cases. The NEB/SQVV found it just for 1-2 and 3-4 minima whereas NEB/L-BFGS did not find any. Figure 3.4 shows the connected paths of the permutations of a LJ_7 cluster as were the result of the NEB and DNEB minimisations.

Figure 3.5 shows a comparison of the NEB and DNEB methods with different optimisers. The graph is the largest magnitude force by the number of force calls in a Pt island rearrangement process [32]. It differs from the iteration measurement because some methods demands two force calls per iteration, such as L-BFGS(line). The convergence stopped when the largest magnitude force reached $10^{-5}eV/$. The NEB/GL-BFGS had the best performance followed by NEB/FIRE, then the swDNEB/L-BFGS(line) and NEB/L-BFGS(line) used the same number of force evaluations. The swDNEB is a method that

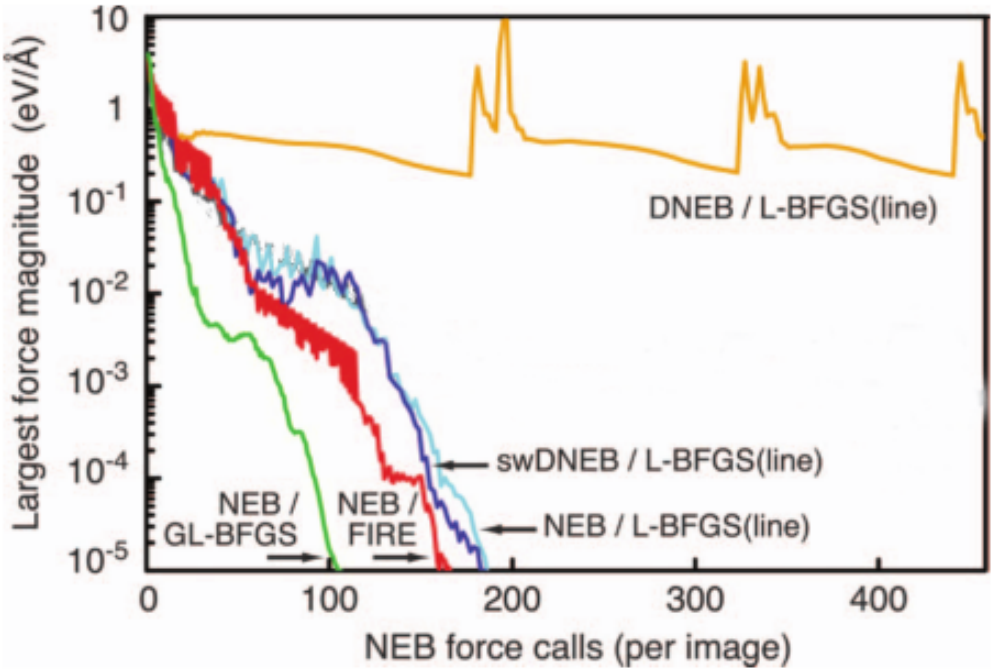

FIGURE 3.5: Largest force magnitude as a function of the force calls per image for a Pt island rearrangement process **??**. It shows the convergence different variations of the NEB method. The swDNEB means that it was switched to NEB to achieve convergence. The image shows that there is no difference between the swDNEB and NEB method in that case, also that NEB/GL-FBGS has a better efficiency followed by NEB/FIRE. The DNEB/L-BFGS demonstrated the instability of the DNEB at low forces (Figure modified from [32]) .

switched from DNEB to NEB when the magnitude of $\mathbf{F}_i^{\perp}$ drops below $\tilde{\mathbf{F}}_i^{\perp}$. On the other hand, DNEB/L-BFGS(line) did not converge due to instability that DNEB presents with low forces. Since this a low force surface, there will be no initial path with high forces to test all DNEB capabilities and efficiency.

3.6 Conclusion

In conclusion, this chapter presented an important chain-of-states method based on an elastic band, the NEB and its variation DNEB, to find MEP and saddle points. Also, it showed that there are several optimisers used to minimise the elastic band with different qualities and speeds. The NEB method with the new tangent definition showed to be a very stable method and useful for most applications. On the other hand, the NEB modification, DNEB, is very good to

high initial forces configurations and it deals well with faster optimisers such as the L-BFGS. It just presents a problem with its exact convergence to the MEP. These double ended methods combined with a tool to find minima give a good overview the PES that can be translated to a disconnectivity graph, as it will be shown in the next chapter.

Chapter 4

Disconnectivity Graphs

4.1 Introduction

The first and second chapters provided a brief introduction of tools that can be used to explore a potential energy surface (PES) by finding minima and transition paths. However, the visualisation of the surface is still not clear. That happens because when the number of atoms, N, increase, thus the number of dimension associated with the surface is 3N+1 (where the extra dimension is the height of the surface) also increase [38].

This hypersurface besides presenting a challenging visualisation problem, has an exponential growth on the number of interesting features, such as minima and transition states. Some solutions were presented. The idea of using one or two hyperdimensions along with the height is not very enlightening and can be misleading. Another visualisation solution was proposed by Kunz and Berry, which is called monotonic sequences [20]. Afterwards, Becker and Karplus introduced the disconnectivity graphs that is known as a powerful method of visualising high dimensional surfaces [2].

It was already used to analyse the PES of several systems such as alanine peptides [21], proteins [25], ferromagnets and spin glasses [12] and clusters [36, 9]. It became popular by its power to provide good insights of the dynamics and thermodynamics of the PES. Also, it allows one to evaluate the relaxation

to the minima, allowing he or she to draw conclusions about the challanges of the process.

4.2 Disconnectivity Graphs

The disconnectivity graphs (see Figure 4.1) use a repository of minima and transition states to be built. The main idea behind the graph is to aggregate the minima according to its proximity. By proximity, I mean the value of the transition state between two minima. So, a pair of minima are close to each other if the value of the transition state is low, whereas they are far if the value is high.

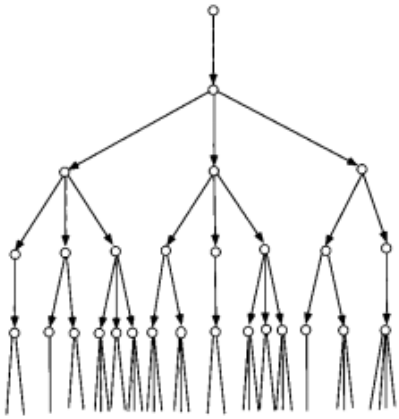

FIGURE 4.1: Disconnectivity graph example where the nodes are represented by hollow circles, each node is a superbasin for what it connects by arrows (below it). The vertical axis represents the energy of the hypothetical surface (Figure from [2]).

To accomplish that, the energy is discretised by a value, ϵ, that is variable. Than, a set of discrete energies $E_1 < E_2 < ... < E_n$, is put in the vertical axis, where E_1 is the lowest energy value that usually resides the global minimum. At each energy, nodes will be put in the horizontal axis. Each node is connect upward and downward by lines to nodes of the neighbouring energies, E_{n-1} and E_{n+1}. At a given node, there are minima that are mutually accessible and can be classified into disjoint sets, this is called 'superbasins'.

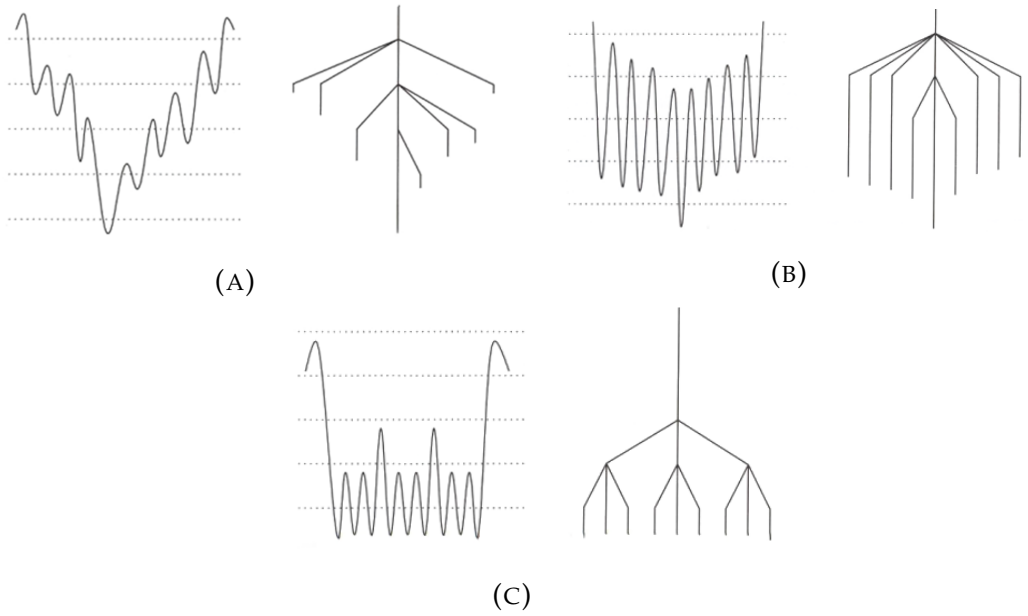

FIGURE 4.2: Disconnectivity graphs of the tree motifs. (A) is the palm tree, (B) the willow tree and (C) the banyan tree(Figures from [2]).

In that way, two minima are said to be in the same 'set' under a superbasin if the lowest transition state between them does not go above the superbasin node. In contrast, they are in different sets if the lowest transition path goes above the threshold. If the energy of the transition path is copiously raised, just one superbasin will remain [2] .

In order to have a good representation of the PES, it is important to set a good value for ϵ. If it is too low, all the transition states will be nodes, a behaviour that overcrowds the graph for large N. On the other hand, if it is too high, the graph will lose a lot of topological information. Although it is a great tool to visualise hypersurfaces of any dimension, it omits important informations such as the density of states.

The disconnectivity graphs can be summarised in three tree motifs (see Figure 4.2). The name tree comes due to the graphs similarity with trees. The 'palm tree' represent a PES that does not have large barriers between its minima, a characteristic that speeds up the relaxation to the minima using a method like the basin hopping. The 'willow tree' has higher energy barriers between its

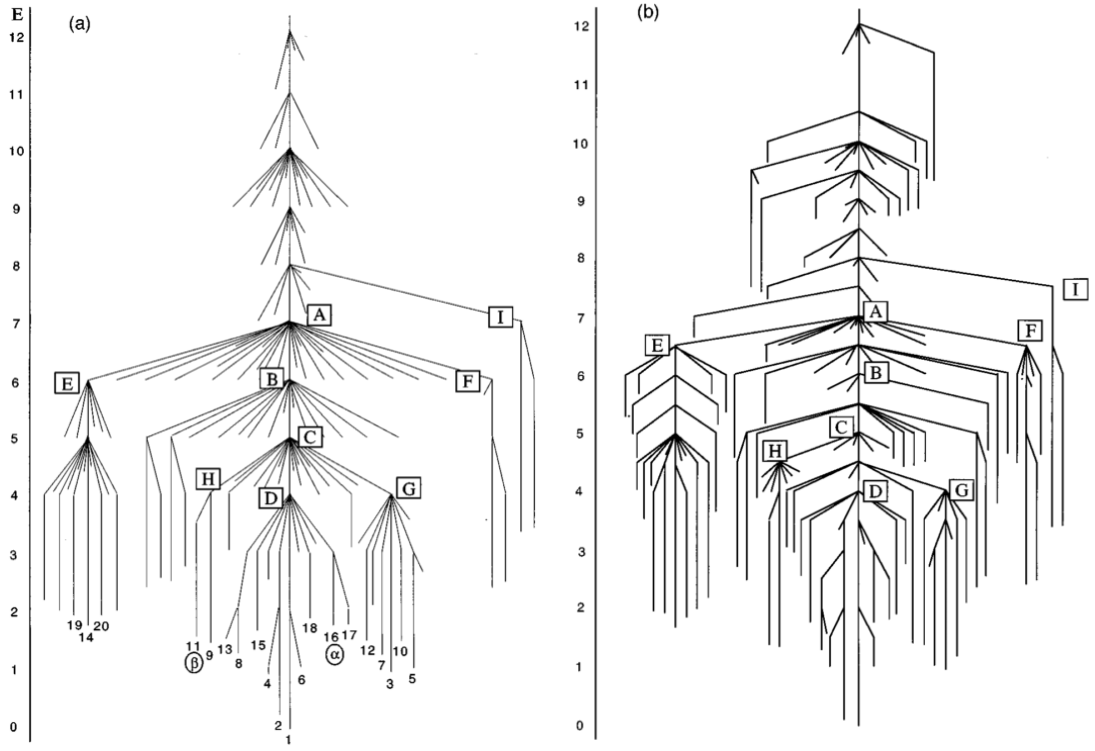

(A) (B)

FIGURE 4.3: Disconnectivity graphs for IAN peptide with energy in kcal/mol. The ϵ in (A) is 2 kcal/mol and 0.5 kcal/mol in (B). The letter at the superbasins are ordered alphabetically for reference. The 20-lowest minima are numbered at (A). (Figures from [2])

minima but the relaxation to the minima is not harder than to the 'banyan tree'. For this one, the barrier between the sets of minima is way bigger than the barrier between a set of minima, what increases the difficulty of finding a global minima. Those motifs do not represent all the possibilities of disconnectivity graphs. But, its ideas and shapes are present on real graphs[2, 38].

To illustrate with a real graph, I will use the first system that used a disconnectivity graph , the IAN tetrapeptide, iso-butyryl-(ala)$_3$-NH-methyl [39, 2]. It had a database of 139 local minima and 502 transition states. The interesting feature of that system is that it is the smallest peptide that presents a α-helical turn.

The graphs on Figure 4.3 have different ϵ. Graph (A), with $\epsilon = 2$ kcal/mol, shows the PES with less resolution, highlighting its global features. With it,

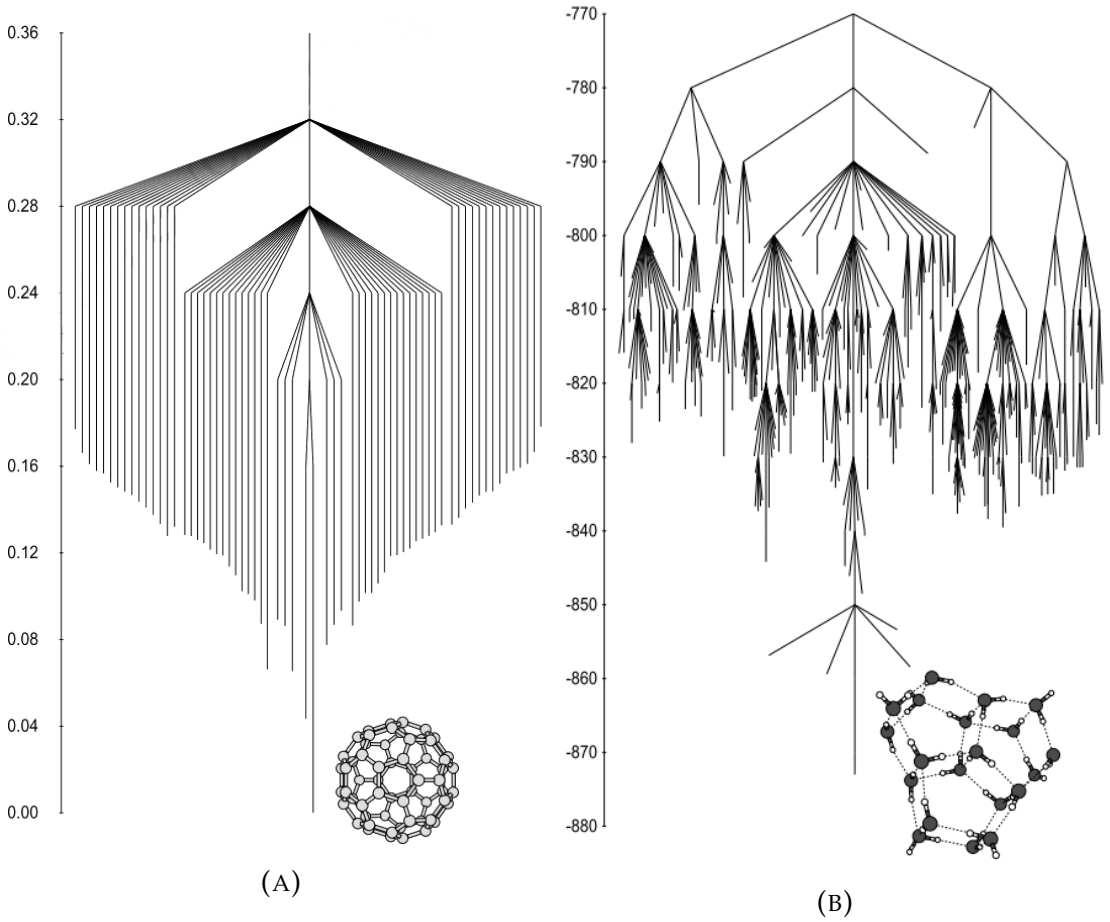

FIGURE 4.4: Disconnectivity graphs of a C_60, buckminsterfullerene, cluster (A) and a $(H_20)_{20}$ cluster (B). The energy of (B) is in kJ mol^{-1}(Figures from [36])

one can observe a funnel-like structure with one brach (E) with considerable size. This branch can be a kinect trap, where the structure can be trapped in a local minima due to the large transition energy demanded to go to the global minima. If graph (B) is considered, its $\epsilon = 0.5$ kcal/mol, hence the definition of the PES will be greater. Thus, some local properties are made clearer.

Some other examples to illustrate the usage of the disconnectivity graphs are in Figure 4.4. The C_60, buckminsterfullerene (Figure 4.4 (A)) is a studied case of molecular simulation [36]. Its energy landscape shows a palm tree structure but with high energy barriers. For that reason, a high temperature is necessary to change the structure of the C_{60}. The other graph, Figure 4.4 (B), is a $(H_20)_{20}$

cluster. It resembles the banyan tree motif, its minima are surrounded by progressively high energy barriers. Hence, the relaxation to the global minimum is hard, since the transition path from one random minimum to the global minimum has a great chance of encountering a high energy barrier.

4.3 Conclusion

This brief chapter presented the powerful idea of the disconnectivity graphs to visualise an hypersurface. By using a repository of minima and transition states it can neatly highlight the important features of an high dimensional surface. It can be used to analyse whether the structure will easily converge to a minima or it can be trapped in a local minima. Also, it exposes the size of the energy barriers between minima, allowing one to do a thermodynamical and dynamical analysis of the transition.

Chapter 5

Lennard Jones Cluster

5.1 Introduction

The Lennard Jones cluster is a system of atoms constructed upon the Lennard Jones potential to mimic a noble gas atoms interaction,

$$V_{ij} = \epsilon(\frac{\sigma}{r_{ij}^{12}} - \frac{\sigma}{r_{ij}^{6}}), \tag{5.1}$$

where V_{ij} is the potential between a pair of atoms ij, r_{ij} is the distance and ϵ and σ are constants. This potential is very useful as a test ground for optimisation techniques for its simplicity and low range reach [39]. It was used to test algorithms that analyse the structure, dynamics and thermodynamics of systems. Empirical investigations even observed some of the minimum configurations predicted by methods.

Due to its use for optimisations, I choose to present examples of the methods that I discussed in the later chapters applied in this system. I will present a remarkable global optimisation example that found up to 110 atoms LJ cluster global minimum, supported by some disconnectivity graphs to illustrate PES. Then, two double ended paths for different sizes cluster.

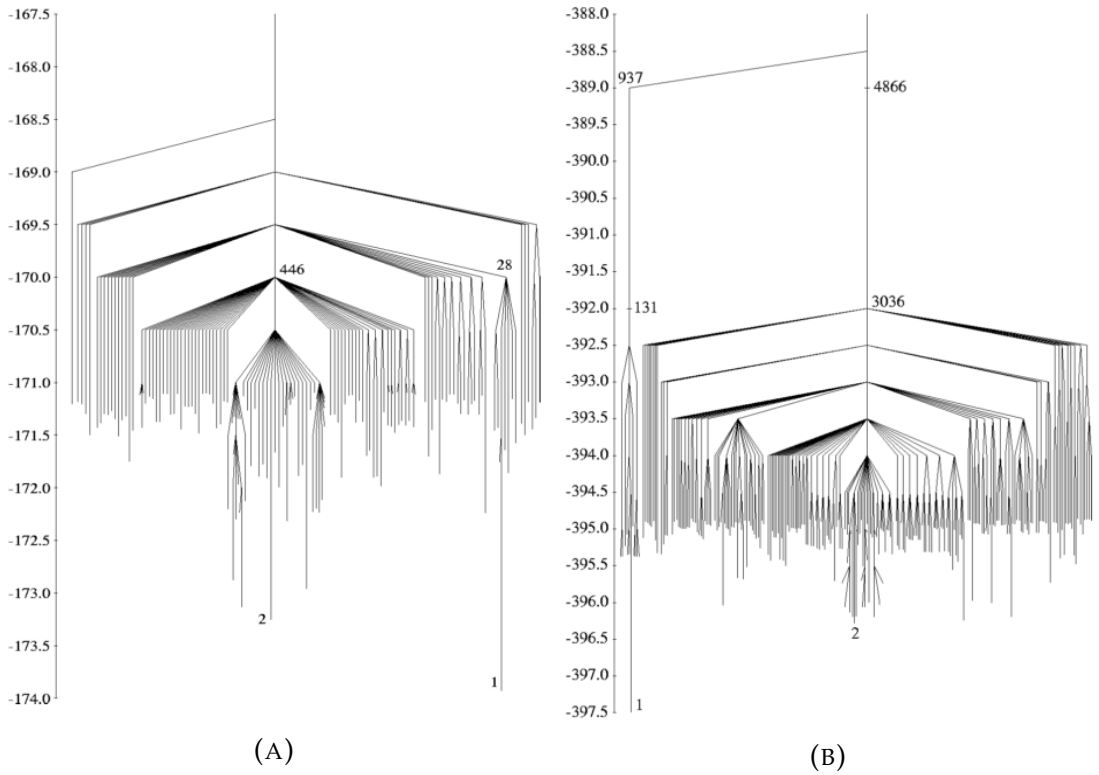

(A) (B)

FIGURE 5.1: Disconnectivity graphs of LJ_38, (A), and LJ_{75}, (B). The graph was done with the lowest minima of each cluster. The numbers on the nodes give the amount of minima in the superbasin.(Figures from [9]).

5.2 Global Optimisation

The paper that introduced the basin hopping algorithm (see Chapter 2), applied it to the Lennard Jones cluster to find the global minimum to systems up to 110 atoms [37]. I will briefly expose the paper's method to find the minima and show, with the help of disconnectivity graphs, minima that were hard to find, LJ_{38} and LJ_{75}.

The original implementation of the basin hopping algorithm used at a constant temperature, $T = 0.8$. The optimiser chosen was the conjugate gradient [28]. Each Monte Carlo step displaced the coordinates of each atom of the cluster $[-1, 1]$ times the step size with an acceptance ration of 0.5. Each of the 110 cluster went through 7 separated runs. The first 5 started from a random generated configurations within a 5.5 reduced units sphere, then suffered 5000

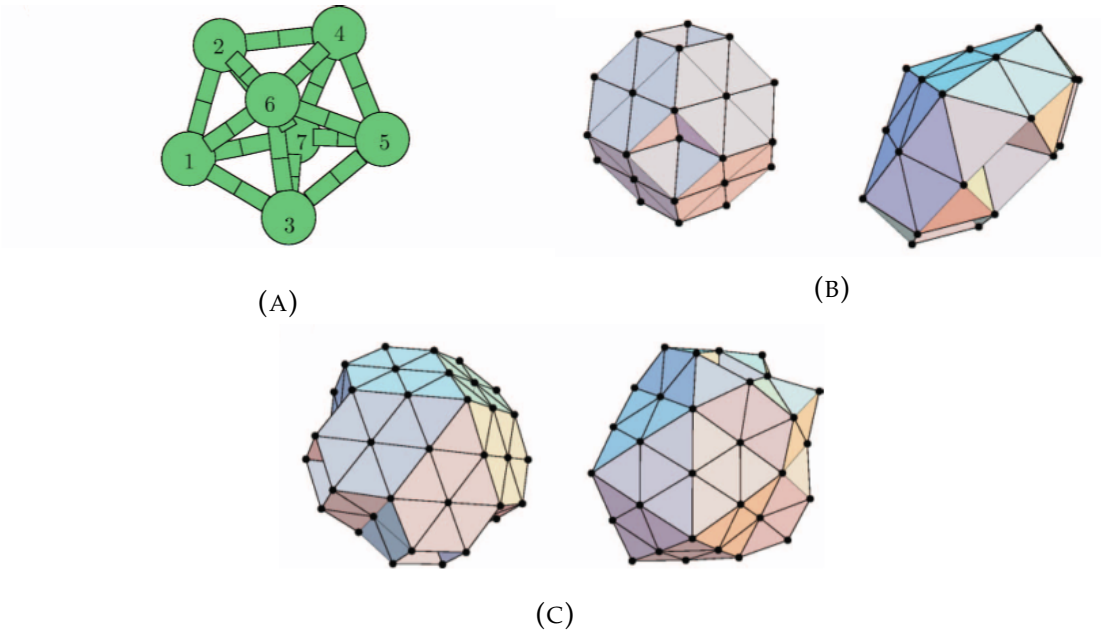

(A) (B)

(C)

FIGURE 5.2: Most stable structures of LJ_7, (A), LJ_38, (B), and LJ_{75}, (C) which were reached by the basin hopping method. The double ended method uses those as endpoints. In the LJ_38 and LJ_{75} the first endpoint is the global minima (right side structures) to the second global minima. For the LJ_7 the endpoints were the same minima with swiped atoms. For instance, the notation 1-2 means that atom 1 was swiped with atom 2.(Figures from [33]).

Monte Carlo steps. The final two had just 200 Monte Carlo steps, but one with one less atom and the other with one more. If it had LJ_{N-1}, N-1 atoms would be frozen for the first 100 steps, whereas an extra atom would suffer angular moves from outside the core. In the case of LJ_{N+1}, the highest energy pair was removed and 200 more unrestricted Monte Carlo moves were applied. It also had a convergence target, if the RMS (root-mean-square) gradient went below 0.01 or the change between the energy of consecutive steps were below 0.1 ϵ, the run ended.

This approach managed to get all the global minima for atoms up to 110 but it also found new minima that were difficult to reach due to its PES. Figure 5.1 shows the disconnectivity graphs for LJ_{38} (A) and LJ_{75}. The graph just shows the lowest energy minima, otherwise the lines would be too dense. In those graphs, the global minimum is not in the main branch of the PES. The overall LJ_{38} PES has a willow tree-like motif where the minima are separated by high

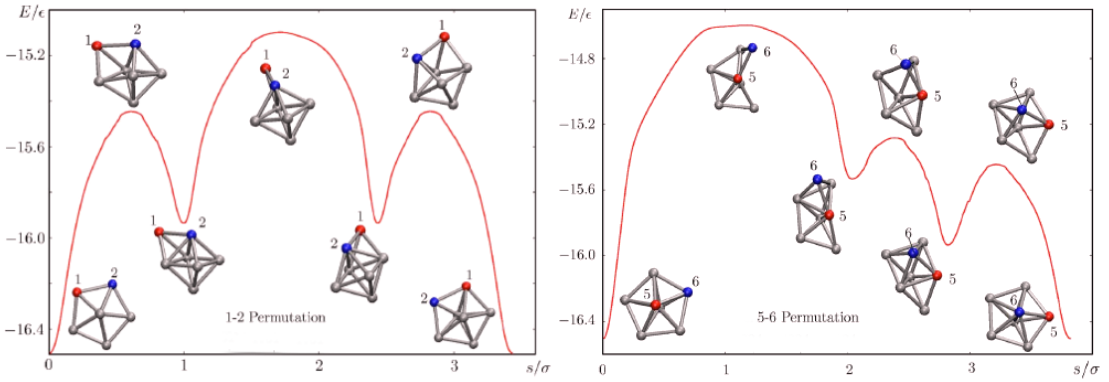

(A) (B)

FIGURE 5.3: Connected paths permutations of the global minima of LJ $_7$ given by the energy as a function of the integrated distance. (A) shows the path for the permutation 5-6 and (B) between 1-2 (Figures modified from [33]).

energy barriers. The global minima is found to be in a branch that has only 28 minima whereas the main branch has 446. Also, in the LJ_{75} case, the whereas the main branch has 4866 minima, the global minimum branch has only 937. In addition, this branches are located in high energy zones, what makes the step for that branch more improbable. This usually makes the search difficult for other types of unbiased searches.

5.3 Transition Path

The double ended method presented on Chapter 3 can be used in LJ clusters analyse its configurations. I will first show a minimum energy path of permutations for the LJ_7 that easily illustrate the process. Then, the MEP between the lowest two minima of LJ_{38} and LJ_{75} [33] .

Figure 5.3 shows the permutation between 1-2 atom, (A), and between 5-6, (B). Both of goes across 3 transition states and 2 local minima. However, the 5-6 permutation has a greater barrier to overcome, -14.7ϵ, than 1-2, -15.2ϵ. This means that permutation of the type 1-2 are easier to happen and demand less energy.

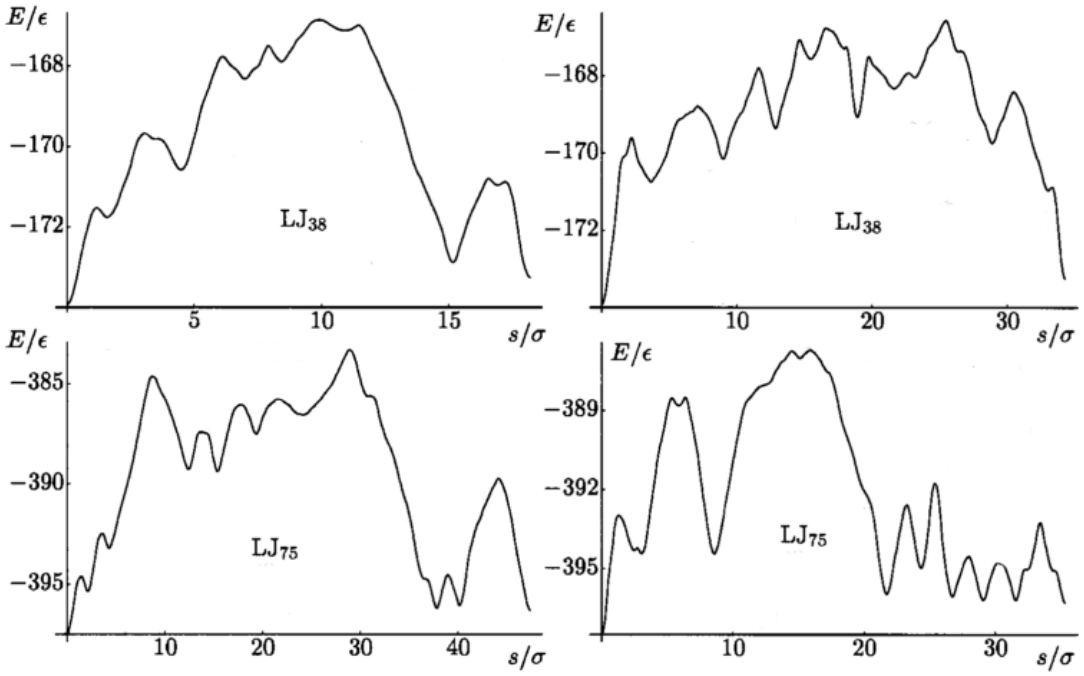

FIGURE 5.4: Connected paths of the two lowest minima LJ_{38} and LJ_{75} with the energy E in function of integrated path length, s.(Figures modified from [33]).

The transition path of LJ_{38} (A) and LJ_{75} (B) at Figure 5.4 shows more transition states what reflects the PES of them. In Figure 5.1, the disconnectivity graphs demonstrates that these two minima are far apart, thus a long transition path between them is necessary. The integrated distance is a measurement of that, for the LJ_7 it has $\sim 3\sigma$ whereas for LJ_{38} it is between $17 \sim 35\sigma$ and between $35 \sim 45\sigma$ for LJ_{75}. The disconnectivity graphs for LJ_{38} and LJ_{75} also says that the energy barrier to be transposed has to have at least -169.5 ϵ and -388.5ϵ, respectively. A statement that is supported by the MEPs which had the maximum transition state for LJ_{38} at -167ϵ and for LJ_{75} it had -386ϵ. This means that the transitions found by the double ended method did not find the most efficient path between those minima.

As a conjecture, one way to possibly find the most efficient path between two minima, i.e. the path that goes through the lowest maximum energy barrier, is to do a basin hopping-like search with a double ended method such as the DNEB. The double ended method is interpolated with a randomly placed

midpoint image and minimised to the connected path. Then, the highest energy barrier point is saved to be compared. In that way, the energy would suffer a modification, $\mathbf{E}(\mathbf{X}) = maxDNEB(\mathbf{E}(\mathbf{X}))$, where $maxDNEB$ means to do a DNEB and select the highest energy value. Thus, it discretises the path in maximum energy barriers (transition states or saddle points). With that modification, the basin hopping algorithm can be applied as in pseudocode 2.2. As a result, the lowest maximum energy barrier can be found.

5.4 Conclusion

In this section, we saw the application of the discussed methods in the latter chapters. The global optimisation used the basin hopping algorithm to find the first 110 minima of LJ clusters. It even found minima of LJ_{38} and LJ_{75} that are hard to localise as shown with the disconnectivity graphs of those. Also, the DNEB was used to find the permutations of LJ_7 defining its transition state structures. The connected paths between the lowest minima of LJ_{38} and LJ_{75} was shown to have a big number of transition states, what agrees with what the disconnectivity graphs has shown. However, the DNEB did not find the best path between its minima, what opens an optimisation oportunity.

Chapter 6

Conclusion

This essay discussed computational methods to survey a potential energy surface. These surfaces are important since they underline the behaviour of several atomic and molecular phenomena such as biomolecules, crystal and glasses.

First, it presented two unbiased methods to find global minimum in combinatorial systems, the simulated annealing and the basin hopping. The former due to its historical importance which is the base for the latter method. The basin hopping proved to be a consistent method to minimise hypersurfaces as one can see in Chapter 5. It managed to find the first 110 minima of LJ clusters including some hard cases, the LJ_{38} and LJ_{75}.

Then, once the minima are found, the double ended methods can be used to localise transition states and the MEP. These states have great importance for dynamical and thermodynamical studies using the hTST theory. The NEB and DNEB are based on the chain of states nudged elastic band concept. The NEB proved to be a very reliable and stable method that can be used in a great variety of situations. DNEB came to solve the instability of NEB along the FBGS optimiser. Thus, it is faster and behaves better at high energy initial situation but appears to not converge tightly.

With the minima and the transition states of a surface a disconnectivity graph can be constructed. It is a very powerful visualisation tool for hypersurfaces that highlights the proximity between minima. Thus, facilitates the

detection of kinetic traps and transition states.

In conclusion, it was shown how a PES can be surveyed with computational tools to provide a description of hypersurfaces.

Bibliography

[1] Jillian Beardwood, J.H. Halton, and J.M. Hammersley. "The shortest path through many points". In: *Mathematical Proceedings of the Cambridge Philosophical Society* 55.04 (1959), pp. 299–327. ISSN: 0305-0041. DOI: 10.1017/S0305004100034095. URL: http://journals.cambridge.org/abstract{_}S0305004100034095.

[2] Oren M. Becker and Martin Karplus. "The topology of multidimensional potential energy surfaces: Theory and application to peptide structure and kinetics". In: *The Journal of Chemical Physics* 106.4 (1997), p. 1495. ISSN: 00219606. DOI: 10.1063/1.473299. URL: http://scitation.aip.org/content/aip/journal/jcp/106/4/10.1063/1.473299.

[3] Erik Bitzek et al. "Structural Relaxation Made Simple". In: *Phys. Rev. Lett.* 97 (17 2006), p. 170201. DOI: 10.1103/PhysRevLett.97.170201. URL: http://link.aps.org/doi/10.1103/PhysRevLett.97.170201.

[4] Joanne M Carr, Semen A Trygubenko, and David J Wales. "Finding pathways between distant local minima." In: *The Journal of chemical physics* 122.23 (2005), p. 234903. ISSN: 0021-9606. DOI: 10.1063/1.1931587. URL: http://www.ncbi.nlm.nih.gov/pubmed/16008483.

[5] Chyung Choi and Ron Elber. "Reaction path study of helix formation in tetrapeptides: Effect of side chains". In: *The Journal of Chemical Physics* 94.1 (1991), p. 751. ISSN: 00219606. DOI: 10.1063/1.460343. URL: http://scitation.aip.org/content/aip/journal/jcp/94/1/10.1063/1.460343.

[6] T E Creighton. “Protein folding.” In: *Biochemical Journal* 270.1 (1990), pp. 1–16. ISSN: 0264-6021. DOI: 10.1016/j.ceb.2011.05.004.

[7] Gordon M. Crippen. “Energy embedding of trypsin inhibitor”. In: *Biopolymers* 21.10 (1982), pp. 1933–1943. ISSN: 1097-0282. DOI: 10.1002/bip.360211002. URL: http://dx.doi.org/10.1002/bip.360211002.

[8] Ryszard Czerminski and Ron Elber. “Self-avoiding walk between two fixed points as a tool to calculate reaction paths in large molecular systems”. In: *International Journal of Quantum Chemistry* 38.S24 (1990), pp. 167–185.

[9] Jonathan P K Doye, Mark A Miller, and David J Wales. “Evolution of the potential energy surface with size for Lennard-Jones clusters”. In: *Journal of Chemical Physycs* 111.18 (1999), pp. 8417–8428. ISSN: 00219606. DOI: 10.1063/1.480217. arXiv: 9903305 [cond-mat]. URL: http://jcp.aip.org/resource/1/jcpsa6/v111/i18/p8417{_}s1.

[10] R. Elber and M. Karplus. “A method for determining reaction paths in large molecules: Application to myoglobin”. In: *Chemical Physics Letters* 139.5 (1987), pp. 375–380. ISSN: 00092614. DOI: 10.1016/0009-2614(87)80576-6. URL: http://www.sciencedirect.com/science/article/pii/0009261487805766.

[11] A Fersht. *Structure and Mechanism in Protein Science: A Guide to Enzyme Catalysis and Protein Folding*. W. H. Freeman, 1999. ISBN: 9780716732686. URL: https://books.google.com.br/books?id=QdpZz{_}ahA5UC.

[12] P Garstecki, T X Hoang, and M Cieplak. “Energy landscapes, supergraphs, and "folding funnels" in spin systems.” In: *Physical review. E, Statistical physics, plasmas, fluids, and related interdisciplinary topics* 60.3 (1999), pp. 3219–

3226. ISSN: 1063-651X. DOI: 10.1103/PhysRevE.60.3219. arXiv: 9904060 [cond-mat].

[13] Fred Glover and Eric Taillard. "A user's guide to tabu search". In: *Annals of operations research* 41.1 (1993), pp. 1–28.

[14] Thomas A. Halgren and William N. Lipscomb. "The synchronous-transit method for determining reaction pathways and locating molecular transition states". In: *Chemical Physics Letters* 49.2 (1977), pp. 225–232. ISSN: 00092614. DOI: 10.1016/0009-2614(77)80574-5. URL: http://www.sciencedirect.com/science/article/pii/0009261477805745.

[15] Graeme Henkelman, Gísli Jóhannesson, and Hannes Jónsson. "METHODS FOR FINDING SADDLE POINTS and Minimum Energy Paths". In: *Theoretical Methods in Condensed Phase Chemistry - Progress in Theoretical Chemistry and Physics - Volume 5* (2002), pp. 269–300. DOI: 10.1007/0-306-46949-9{_}10. URL: http://doi.org/10.1007/0-306-46949-9{_}10.

[16] Graeme Henkelman and Hannes Jónsson. "Improved tangent estimate in the nudged elastic band method for finding minimum energy paths and saddle points". In: *Journal of Chemical Physics* 113.22 (2000), pp. 9978–9985. ISSN: 00219606. DOI: 10.1063/1.1323224.

[17] Luc Jaulin. *Applied interval analysis: with examples in parameter and state estimation, robust control and robotics*. Vol. 1. Springer Science & Business Media, 2001.

[18] Hannes Jonsson, Greg Mills, and Karsten W. Jacobsen. "Nudged elastic band method for finding minimum energy paths of transitions". In: *Classical and Quantum Dynamics in Condensed Phase Simulations - Proceedings of the International School of Physics*. 1998, pp. 385–404. ISBN: 9789810234980. DOI: 10.1142/9789812839664{_}0016.

[19] S Kirkpatrick, C D Gelatt, and M P Vecchi. "Optimization by Simulated Annealing". In: *Science* 220.4598 (1983), pp. 671–680. ISSN: 00368075. DOI: 10.1126/science.220.4598.671. URL: http://www.jstor.org/stable/1690046.

[20] Ralph E Kunz and R Stephen Berry. "Statistical interpretation of topographies and dynamics of multidimensional potentials". In: *The Journal of Chemical Physics* 103.5 (1995), p. 1904. ISSN: 00219606. DOI: 10.1063/1.469714. URL: http://link.aip.org/link/?JCP/103/1904/1.

[21] Y Levy and O M Becker. "Effect of conformational Constraints on the Topography of Complex Potential Energy Surfaces". In: *Phys. Rev. Lettr.* 81.5 (1998), pp. 1126–1129. ISSN: 0031-9007. DOI: 10.1103/PhysRevLett.81.1126.

[22] P. Maragakis et al. "Adaptive nudged elastic band approach for transition state calculation". In: *The Journal of Chemical Physics* 117.10 (2002), p. 4651. ISSN: 00219606. DOI: 10.1063/1.1495401. URL: http://scitation.aip.org/content/aip/journal/jcp/117/10/10.1063/1.1495401.

[23] Kenneth Merz and Scott M LeGrand. *The protein folding problem and tertiary structure prediction*. Springer Science & Business Media, 2012.

[24] Nicholas Metropolis et al. "Equation of State Calculations by Fast Computing Machines". In: *The Journal of Chemical Physics* 21.6 (1953), pp. 1087–1092. ISSN: 00219606. DOI: doi:10.1063/1.1699114. arXiv: 5744249209. URL: http://jcp.aip.org/resource/1/jcpsa6/v21/i6/p1087{_}s1?bypassSSO=1.

[25] Ma Miller and Dj Wales. "Energy landscape of a model protein". In: *The Journal of chemical physics* 111.14 (1999), pp. 6610–6616. ISSN: 0021-9606, 1089-7690. DOI: 10.1063/1.480011. arXiv: 9904304v1 [arXiv:cond-mat].

URL: http://scitation.aip.org/content/aip/journal/jcp/111/14/10.1063/1.480011$\backslash$nhttp://link.aip.org/link/?JCPSA6/111/6610/1.

[26] J N Murrell and K J Laidler. "Symmetries of activated complexes". In: *Trans. Faraday Soc.* 64.0 (1968), pp. 371–377. DOI: 10.1039/TF9686400371. URL: http://dx.doi.org/10.1039/TF9686400371.

[27] Jorge Nocedal. "Updating quasi-Newton matrices with limited storage". In: *Mathematics of computation* 35.151 (1980), pp. 773–782.

[28] WH Press et al. "Numerical Recipes (Cambridge University, Cambridge, 1986)". In: *Chap* 9 (1990), pp. 243–246.

[29] Sigurd Schelstraete and Henri Verschelde. "Finding minimum-energy configurations of Lennard-Jones clusters using an effective potential". In: *The Journal of Physical Chemistry* 5639.96 (1997), pp. 310–315. ISSN: 1089-5639. DOI: 10.1021/jp9621181. URL: http://pubs.acs.org/doi/abs/10.1021/jp9621181.

[30] Pablo Serra, Aaron F. Stanton, and Sabre Kais. "Pivot method for global optimization". In: *Phys. Rev. E* 55 (1 1997), pp. 1162–1165. DOI: 10.1103/PhysRevE.55.1162. URL: http://link.aps.org/doi/10.1103/PhysRevE.55.1162.

[31] Daniel Sheppard and Rye Terrell. *Saddle Point Finding Methods*. URL: http://theory.cm.utexas.edu/henkelman/research/saddle/ (visited on 11/09/2015).

[32] Daniel Sheppard, Rye Terrell, and Graeme Henkelman. "Optimization methods for finding minimum energy paths." In: *The Journal of chemical physics* 128.13 (2008), p. 134106. ISSN: 0021-9606. DOI: 10.1063/1.2841941.

[33] Semen a. Trygubenko and David J. Wales. "A doubly nudged elastic band method for finding transition states (Journal of Chemical Physics (2004) 120 (2082))". In: *Journal of Chemical Physics* 120.16 (2004), p. 7820. ISSN: 00219606. DOI: 10.1063/1.1691408. arXiv: 0402209 [cond-mat].

[34] Chiachin Tsoo and Charles L. Brooks. "Cluster structure determination using Gaussian density distribution global minimization methods". In: *The Journal of Chemical Physics* 101.8 (1994), p. 6405. ISSN: 00219606. DOI: 10.1063/1.468397. URL: http://scitation.aip.org/content/aip/journal/jcp/101/8/10.1063/1.468397.

[35] A. ULITSKY and R. ELBER. "A new technique to calculate steepest descent paths in flexible polyatomic systems". eng. In: *The Journal of chemical physics* 92.2 (), pp. 1510–1511. ISSN: 0021-9606. URL: http://cat.inist.fr/?aModele=afficheN{\&}cpsidt=6804969.

[36] D J Wales, M a Miller, and T R Walsh. "Archetypal energy landscapes". In: *Nature* 394.6695 (1998), pp. 758–760. ISSN: 0028-0836. DOI: 10.1038/29487. URL: http://www.nature.com/doifinder/10.1038/29487$\backslash$npapers3://publication/doi/10.1038/29487.

[37] David Wales and Jonathan P. K. Doye. "Global Optimization by Basin-Hopping and the Lowest Energy Structures of Lennard-Jones Clusters Containing up to 110 Atoms". In: *Journal of Physical Chemistry A* 101.97 (1997), pp. 5111–5116. ISSN: 1089-5639. DOI: 10.1021/jp970984n. arXiv: 9803344 [cond-mat]. URL: http://arxiv.org/abs/cond-mat/9803344.

[38] David J Wales. "Energy Landscapes: From Clusters to Supercooled Liquids and Glasses". In: (2008).

[39] David J Wales. "Energy Landscapes: From Clusters to Supercooled Liquids and Glasses". In: (2008).